Progress In Electromagnetics Research C, Vol. 119, 31–47, 2022

A New Fault Location Method Independent of Line Parameters

Lihui Zhao[1, 2], Jingwei Zhu[1, *], Hongzhe Yang[2], and Bin Gu[1]

Abstract—To restore power feeding as soon as possible and reduce repair costs and labor, a precise and robust fault location method for transmission lines is proposed. This method is based on the current and voltage synchronously collected by the phasor measurement units (PMUs) at two terminals of the line and does not require line parameters to calculate the fault distance. The line parameter is not approximately constant, but is affected by power load, temperature, and humidity, which affects the accuracy of most fault location algorithms that rely on line parameters. Therefore, the method proposed in this paper is robust and accurate. The method is based on the sequence fault component network and synchronous measurement technology, which is not affected by the system's pre-fault state, fault type, fault inception angle, and fault phase. Then, the method is verified in PSCAD/EMTDC by choosing different path resistances, fault types, fault inception angles, load currents, and line transpositions. A large number of simulation results show that the proposed method has high accuracy and robustness.

1. INTRODUCTION

With the development of society and growth of economic activities, power grid has played an increasingly important role. In order to meet the needs of society, the voltage level and capacity of the power grid are also increasing. Among many protection devices in the power grid, fault location equipment can calculate the distance from the reference point to the fault point. When faults occur, in order to reduce labor costs and restore power as soon as possible, it is necessary to develop a more accurate and faster fault location method. In the past two decades, related fault location techniques have been proposed in the literatures.

The fault location of transmission lines can be divided into three categories [1]: fault analysis algorithm, traveling wave location algorithm [2, 3], and intelligent location algorithm according to different location principles [4–6]. Fault analysis method requires the relevant system parameters and voltage and current to be obtained by line measuring device. According to different sources of line parameter acquired, it is divided into single terminal method and two terminals method [7, 8].

Single terminal fault location method calculates the distance through the impedance of the transmission from measuring terminal to fault point. This algorithm requires that the parameters include voltage and current measured from one end, line impedance, zero sequence impedance, and path resistance [9, 10]. Therefore, the single terminal method is relatively simple and easy to implement but not accurate. The zero-sequence impedance needs to be known in advance but is difficult to obtain accurately and is affected by the path resistance and line parameters. Obviously, the advantage of the algorithm in this paper is that it does not require zero-sequence components and line parameters in the derivation process. The algorithm does not require zero sequence data to locate the fault.

The two terminals fault location method is not affected by the path resistance, and it does not need to judge the fault type [11–13]. Compared with the single-terminal method, the two-terminal

Received 11 January 2022, Accepted 28 February 2022, Scheduled 9 March 2022

* Corresponding author: Jingwei Zhu (zjwdl@dlmu.edu.cn).

[1] College of Marine Electrical Engineering, Dalian Maritime University, Dalian 116026, China. [2] School of Electrical Engineering, Shanghai Institute of Technology, Shanghai, China.

method tends to have higher accuracy. The method needs to obtain the information of the measuring devices at both ends of the line, so it requires advanced communication technology and complicated device. Data sampling at both ends can be either synchronized or unsynchronized [14–17]. Synchronous data sampling increases the complexity of the algorithm, but the positioning accuracy is high, and synchronization algorithms are also required. Asynchronous sampling reduces the complexity of the algorithm, but the positioning accuracy is reduced, and asynchronous algorithm is required. With the development of communication technology, it is more convenient and reliable to obtain data at both ends simultaneously.

Jiang et al. [18] have proposed a single terminal fault distance method, which uses phase current and voltage calculation at one end. Liao [19] has developed a positioning method that uses data at both ends and requires data synchronization. Yu et al. [20] has proposed a positioning method for series compensation lines. Liao and Elangovan [21] have proposed a technique for fault location, using asynchronous data at two terminals or three terminals. Feng and Abur [22] have proposed a fault location technique for transmission lines using Kalman filter. Zhao et al. [23] have developed fault location technique based on two terminals. The algorithm is accurate but requires line parameters, and does not consider the effects of parameter changes on the calculation results.

The above-mentioned fault location methods all need to know line parameters and line length in advance. However, line parameters, especially zero sequence parameters, are not always known. Even if available, the line parameters can vary with temperature, humidity, and load. Therefore, inaccurate parameters may affect the location accuracy of the algorithms.

Zhang et al. [24] and Liao [25] have proposed the fault location algorithm that does not require line parameters. The algorithm only uses voltage and current to solve asymmetric fault location.

The algorithm proposed in this paper can locate various faults without prefault data. The algorithm only uses positive and negative sequence fault components and does not require zero sequence components, so it is not affected by zero sequence coupling. The algorithm uses the voltage and current measured at both ends, evolved from synchronous data sampling. The algorithm does not require a high sampling frequency, compared to the fault location method based on the traveling wave principle.

This paper describes in detail the data sampling, transformation, fault component extraction, and location algorithm in Section 2. For different fault types, path resistances, fault inception angles, line transpositions, and line loads, a large number of simulations are carried out with PSCAD in Section 3.

2. DERIVATION OF THE FAULT LOCATION ALGORITHM

In this section, a precise fault location for transmission lines independent of line parameters is presented. The detailed evolution process for asymmetrical and three-phase short-circuit faults is given. The algorithm implementation steps are as follows.

(1) Obtain the instantaneous values of the three-phase voltage and current on both sides of the transmission line;

(2) Perform fault component extraction and obtain the fault components of the three-phase voltage and current on both sides of the line;

(3) Differentially filter the fault component of the three-phase current to suppress the attenuated DC component in the fault current;

(4) Obtain the corresponding fundamental frequency phasor component through full-wave Fourier transform;

(5) Achieve amplitude and phase compensation for the fundamental frequency component of the fault;

(6) Filter sequence to obtain the positive and negative sequence fault components of the voltage and current on both sides of the line.

2.1. System Description

Figure 1 illustrates the single-line diagram of the selected 200 km, 500 kV transmission line. The PMU is installed at both ends of the line to measure the instantaneous values of the three-phase voltage and current, where

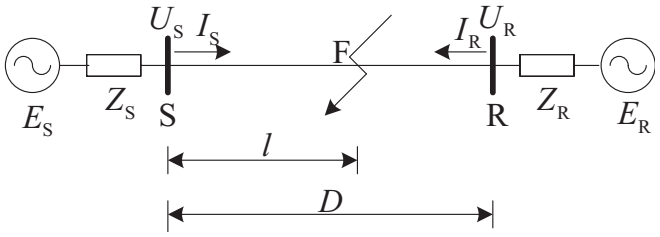

Figure 1. Single-line diagram of transmission line.

F fault location,
S sending end of the line,
R receiving end of the line,
D transmission line length,
l fault distance.

In Fig. 2, different short-circuit faults with path resistance are shown. The algorithm in this paper solves the problem of fault location for asymmetric short-circuit and three-phase short-circuit (TPH). Asymmetric short circuits include double-phase short circuits (DPH), single-phase to ground short circuits (SPG), and double-phase to ground short circuits (DPG).

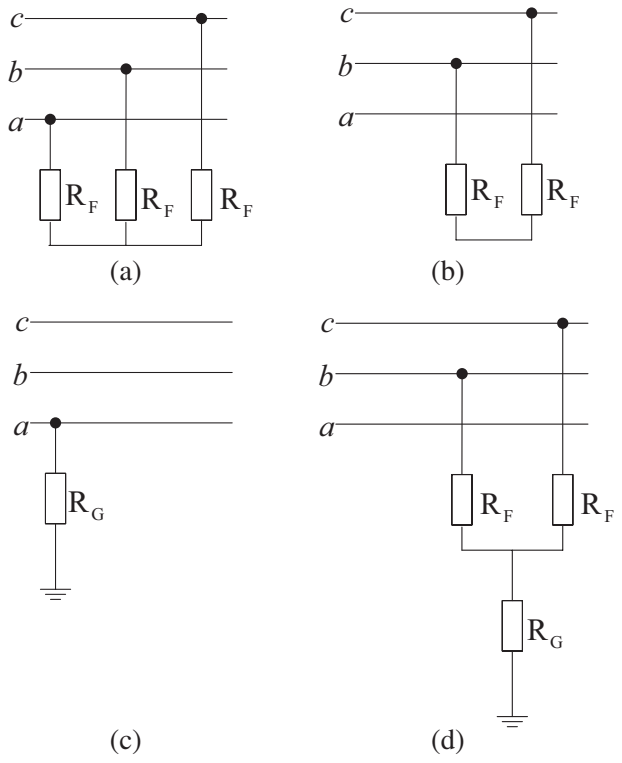

Figure 2. Different fault diagrams. (a) TPH. (b) DPH. (c) SPG. (d) DPG.

2.2. Fundamental Frequency Phasor Component and Sequence Fault Component

In order to reduce the detection error of system oscillation and frequency offset, Equation (1) is used to extract the fault component.

$$\Delta f(k) = [f(k) - f(k-2N)] - [f(k-2N) - f(k-4N)] \tag{1}$$

where f is defined as electrical physical quantities such as voltage or current, and N is the number of sampling points per cycle.

Using the fault extraction method of Equation (1), the current of the fault extraction algorithm proposed is smaller, which reduces the detection error of system oscillation and frequency offset. The detailed deduction process is described in the literature [23].

Differential filtering performs amplitude and phase compensation for the current phasor of the fault component. Differential filtering is as follows:

$$d\Delta i(t) = \Delta i(t) - \Delta i(t - \Delta T) \tag{2}$$

where $\Delta i(t)$ is the instantaneous value of three-phase fault component current, and $d\Delta i(t)$ is the instantaneous value of three-phase fault component current after differential filtering. ΔT is the sampling period.

From Taylor series, Equation (2) can be rewritten as:

$$\begin{aligned} d\Delta i(t) &= \Delta i(t) - \Delta i(t - \Delta T) \\ &= I_0 e^{-\frac{t}{\tau}} + I_{m1} \sin(\omega t + \theta_1) - \left[I_0 e^{-\frac{(t-\Delta T)}{\tau}} + I_{m1} \sin(\omega t + \theta_1 - \omega \Delta T) \right] \\ &\approx -\frac{1}{\tau f_s} I_0 e^{-\frac{t}{\tau}} + 2 I_{m1} \sin\left(\frac{\pi}{N}\right) \sin\left[(\omega t + \theta_1) + \frac{\pi}{2} - \frac{\pi}{N} \right] \end{aligned} \tag{3}$$

where τ is the time constant, I_{m1} the AC component amplitude of current fault component, and N the number of sampling points per cycle. From Equation (3), the DC component is very small.

Fault phase components equation is the following:

$$\Delta U_1 = \frac{1}{3} \left(\Delta U_a + \alpha \Delta U_b + \alpha^2 \Delta U_c \right) \tag{4}$$

$$\Delta I_1' = \frac{1}{3} \left(d\Delta I_a + \alpha d\Delta I_b + \alpha^2 d\Delta I_c \right) \tag{5}$$

where $\alpha = \exp(j2\pi/3)$.

The amplitude and phase angle of the wave after the differential filter are different from that of the initial wave. Equation (6) is valid when the sampling frequency is 2000 Hz. Amplitude and phase compensation Equation is as follows:

$$\Delta_1 = \Delta I_1' \cdot 6.37 \angle (-85.5^\circ) \tag{6}$$

where $\Delta I_1'$ is the phasor form corresponding to Equation (3). The amplitude ratio is 6.37, and the phase difference is -85.5°.

2.3. Asymmetrical Fault Algorithm

Through the above-mentioned digital processing process, the positive sequence, negative sequence, and zero sequence fault components of voltage and current are calculated. For asymmetric short-circuit faults, this algorithm only uses positive sequence and negative sequence fault components. Therefore, the transmission line shown in Fig. 1 can be represented by sequence component networks, including: positive (1), negative (2), and zero (0). The positive sequence and negative sequence component network diagrams used in the algorithm are shown in Figs. 3 and 4.

In Figs. 3 and 4, the voltage balance equation is as follows:

$$\Delta \dot{U}_{S1} - zl\Delta \dot{I}_{S1} = \Delta \dot{U}_{R1} - z(D-l)\Delta \dot{I}_{R1} \tag{7}$$

$$\dot{U}_{S2} - z_1 l \dot{I}_{S2} = \dot{U}_{R2} - z(D-l)\dot{I}_{R2} \tag{8}$$

where $\Delta \dot{U}_{S1}$, $\Delta \dot{U}_{S2}$ are respectively positive and negative sequence fault phase voltages at the bus on the sending side; $\dot{U}_{R1}$, $\dot{U}_{R2}$ are respectively positive and negative sequence fault phase voltages at the bus on the receiving side; $\Delta \dot{I}_{S1}$, $\Delta \dot{I}_{S2}$ are respectively positive and negative sequence fault phase currents at the bus on the sending side; $\dot{I}_{R1}$, $\dot{I}_{R2}$ are respectively positive and negative sequence fault phase currents at the bus on the receiving side; z is the line impedance per unit length.

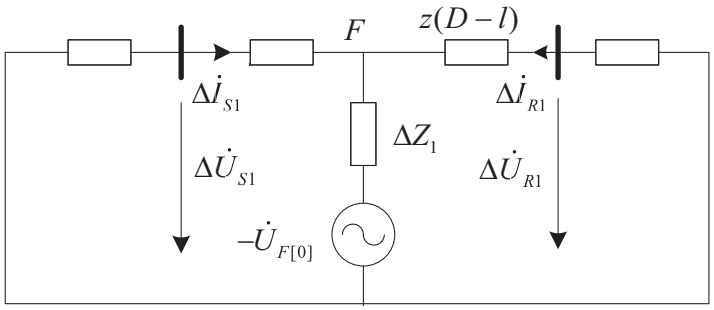

Figure 3. Positive sequence fault component network diagram.

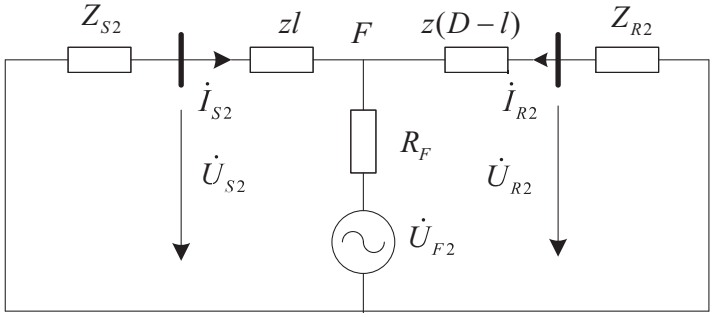

Figure 4. Negative sequence fault component network diagram.

From Equations (7) and (8), the fault location solution is as follows:

$$zl = \frac{\left(\Delta\dot{U}_{S1} - \Delta\dot{U}_{R1}\right)\dot{I}_{R2} - \left(\dot{U}_{S2} - \dot{U}_{R2}\right)\Delta\dot{I}_{R1}}{\Delta\dot{I}_{S1}\dot{I}_{R2} - \dot{I}_{S2}\Delta\dot{I}_{R1}} \tag{9}$$

$$z(D-l) = \frac{\left(\Delta\dot{U}_{S1} - \Delta\dot{U}_{R1})\dot{I}_{S2} - \left(\dot{U}_{S2} - \dot{U}_{R2}\right)\Delta\dot{I}_{S1}\right.}{\Delta\dot{I}_{S1}\dot{I}_{R2} - \dot{I}_{S2}\Delta\dot{I}_{R1}} \tag{10}$$

In order to find a fault location solution independent of line parameters, l is expressed as a percentage of D

$$l\% = \frac{100zl}{zl + z(D-l)} \tag{11}$$

An equation independent of line parameters is obtained by substituting Eqs. (9) and (10) into Eq. (11). Then the fault distance can be obtained as follows:

$$l\% = 100\frac{\left(\Delta\dot{U}_{S1} - \Delta\dot{U}_{R1}\right)\dot{I}_{R2} - \left(\dot{U}_{S2} - \dot{U}_{R2}\right)\Delta\dot{I}_{R1}}{\left(\Delta\dot{U}_{S1} - \Delta\dot{U}_{R1}\right)\left(\dot{I}_{S2} + \dot{I}_{R2}\right) - \left(\dot{U}_{S2} - \dot{U}_{R2}\right)\left(\Delta\dot{I}_{S1} + \Delta\dot{I}_{R1}\right)} \tag{12}$$

For asymmetric faults, only the positive sequence and negative sequence components are used, and the result of fault location is more accurate. Path resistance is not used in Equation (12), and it will not affect the result of location.

2.4. Three-Phase Fault Algorithm

For symmetric faults, there is no negative sequence component, which limits the application of Equation (12).

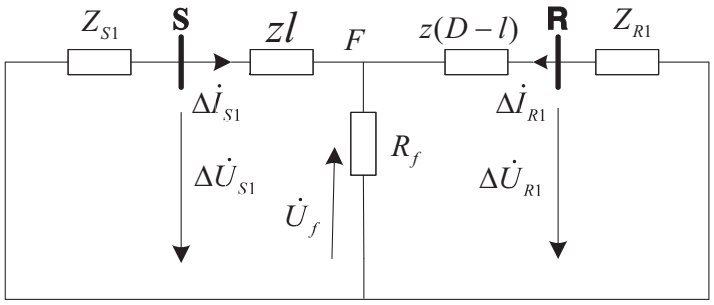

Figure 5. Positive sequence fault component network diagram of three-phase failure.

In Fig. 5, the voltage balance equation is as follows

$$\Delta\dot{U}_{S1} - zl\Delta\dot{I}_{S1} = \dot{U}_f \tag{13}$$

$$\Delta\dot{U}_{R1} - z(D-l)\Delta\dot{I}_{R1} = \dot{U}_f \tag{14}$$

For three phase faults, Equations (13) and (14) can be rewritten as

$$zl = \frac{\Delta\dot{U}_{S1} - \dot{U}_f}{\Delta\dot{I}_{S1}} \tag{15}$$

$$z(D-l) = \frac{\Delta\dot{U}_{R1} - \dot{U}_f}{\Delta\dot{I}_{R1}} \tag{16}$$

By substituting Eqs. (15) and (16) into Eq. (11), l is expressed as a percentage of D, and the fault distance is as follows:

$$l\% = 100\frac{\left(\Delta\dot{U}_{S1} - \dot{U}_f\right)\Delta\dot{I}_{R1}}{\left(\Delta\dot{U}_{S1} - \dot{U}_f\right)\Delta\dot{I}_{R1} + \left(\Delta\dot{U}_{R1} - \dot{U}_f\right)\Delta\dot{I}_{S1}} \tag{17}$$

When a metallic three-phase short circuit occurs, the voltage at fault point is zero. Equation (17) can be rewritten as

$$l\% = 100\frac{\Delta\dot{U}_{S1}\Delta\dot{I}_{R1}}{\Delta\dot{U}_{S1}\Delta\dot{I}_{R1} + \Delta\dot{U}_{R1}\Delta\dot{I}_{S1}} \tag{18}$$

When a three-phase short circuit with arc and path resistance occurs, the voltage at the fault point cannot be ignored. The voltage at fault point in Equation (18) is not available. In this case, the algorithm will produce errors. The subsequent simulation of the algorithm gives errors. As for the asynchronous errors in data sampling, they will occur at both ends of the line when the three-phase short circuit occurs. This means that the phase voltage and current of Equation (18) are not affected by synchronization errors.

For asymmetric faults and three-phase faults given above, the algorithm given above does not require prior knowledge of the fault type and fault phase. When a negative sequence component is detected, it can be known that an asymmetric fault has occurred.

3. PERFORMANCE EVALUATION

An overhead transmission line model is built in PSCAD/EMTDC to validate the algorithm. From Fig. 1, the voltage level is 500 kV, and the line length is 400 km. The parameters of the simulation model are shown in Table 1. The line parameters are shown in Table 2.

Table 1. Parameters of the simulation model.

Parameters	System (S)	System (R)
$U_{LL,RMS}$ [kV]	515	500
ϕ_1 [°]	0	−15
R [Ω]	0.013	0.005
L [H]	0.0752	0.0623
R_0 [Ω]	4.5123	3.5610
L_0 [H]	0.0865	0.5631

Table 2. Line parameters.

Parameters	p- and n-sequence	0-sequence
Resistance Ω/km	0.0210	0.152
Inductance mH/km	0.872	2.985
Capacitance μF/km	0.015	0.007

3.1. Asymmetrical Fault Evaluation

In this section, Equation (12) is used to carry out a large number of tests for asymmetric faults including metallic faults and faults with transition resistance. The types of failures tested include DPG, DPH, and SPG. The point of failure is set to 60 km away from the sender. The fault initiation time is $t = 20$ ms. The simulation adopts synchronous sampling, and the sampling frequency is 2 kHz.

The different metallic asymmetry faults are shown in Fig. 6 to Fig. 8. From the simulation results, the fault location distance can be correctly calculated within 20 ms for metallic asymmetry faults.

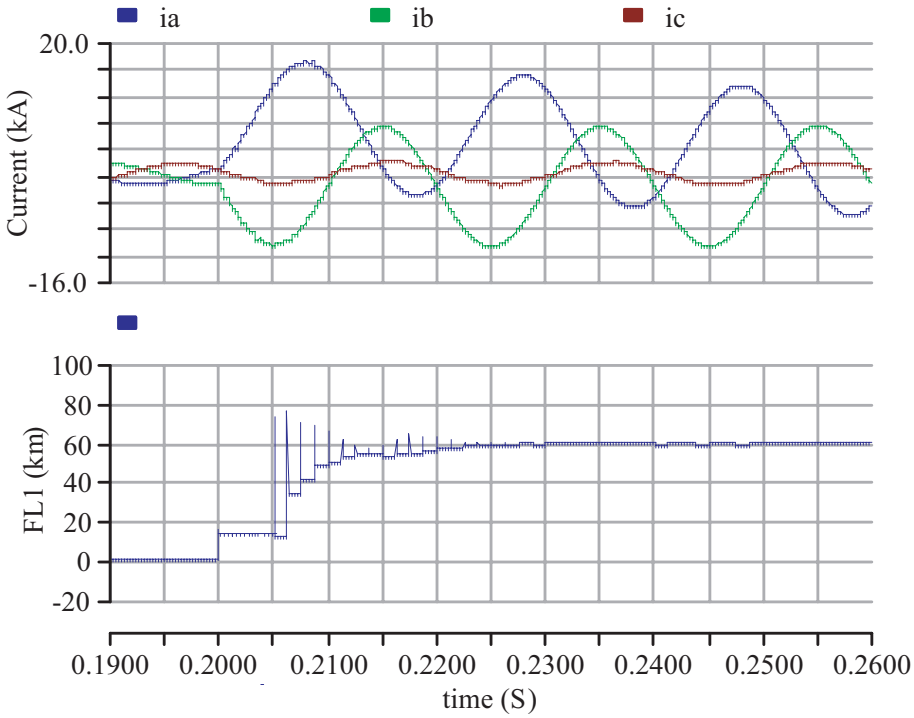

Figure 6. Metallic DPG.

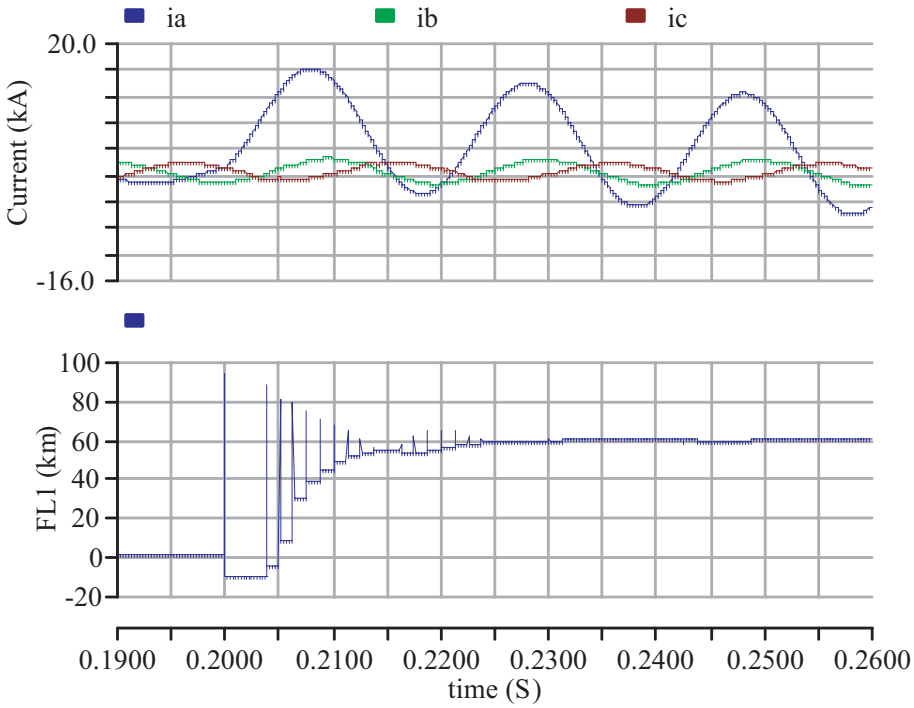

Figure 7. Metallic SPG.

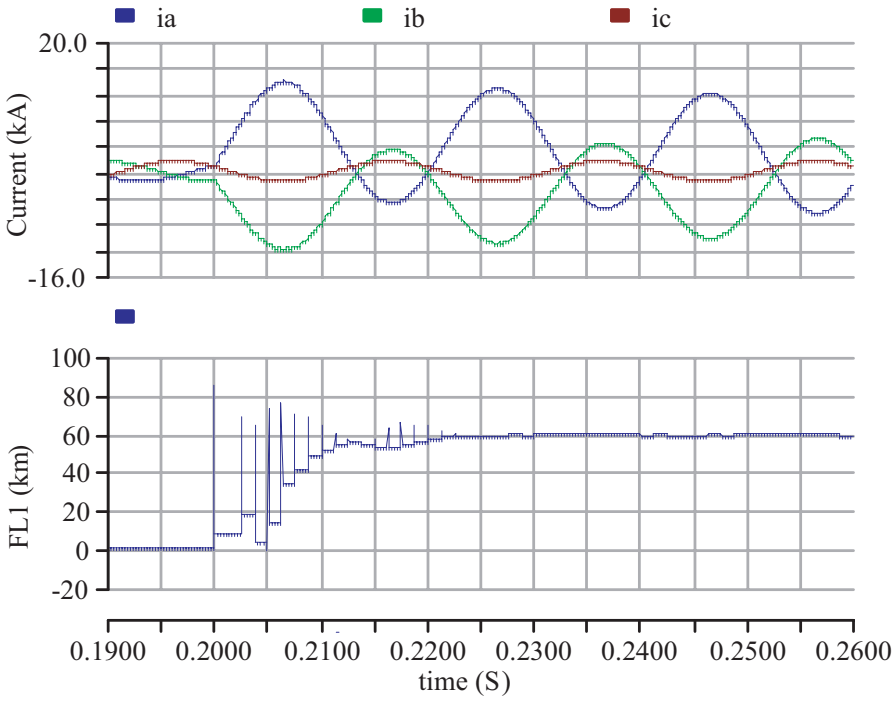

Figure 8. Metallic DPH.

The different asymmetry faults with path resistance $R_f = 30\,\Omega$ are shown in Fig. 9 to Fig. 11. From the simulation results, the algorithm has nothing to do with transition resistance.

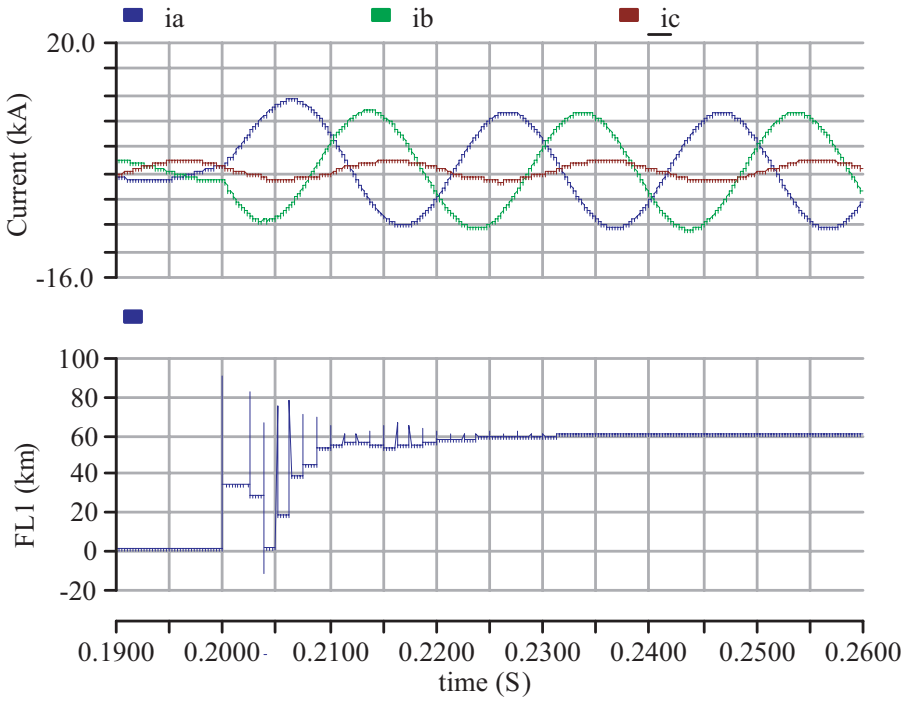

Figure 9. DPG with transition resistance $R_f = 30\,\Omega$.

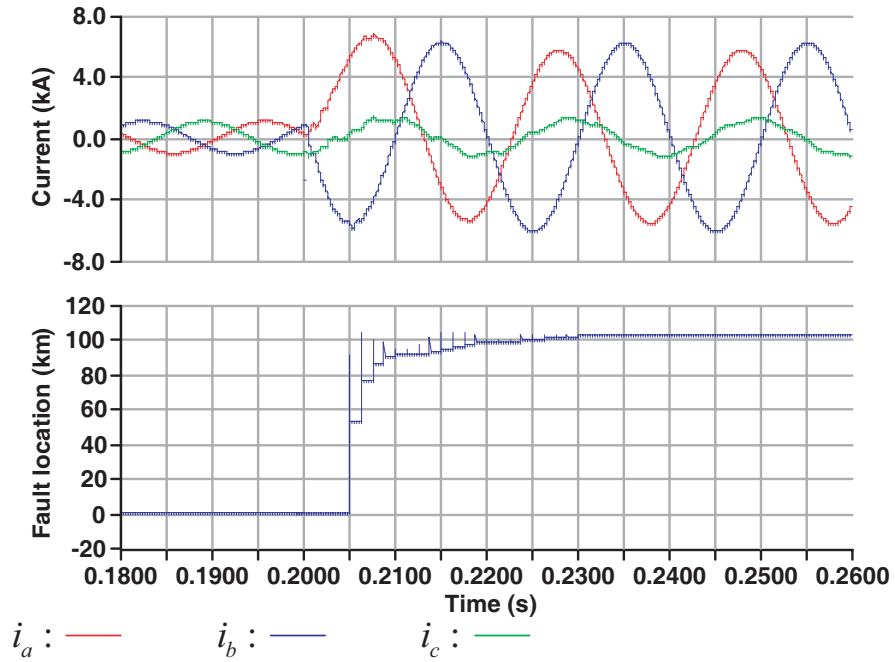

Figure 10. DPH with transition resistance $R_f = 30\,\Omega$.

3.2. Symmetrical Fault Evaluation

The fault start time, sampling frequency, system and line parameters, and fault points are the same as asymmetric faults. Symmetrical fault simulation uses Equation (18) to calculate the distance to fault.

Figure 12 shows the fault location current and fault distance under a metallic three-phase short

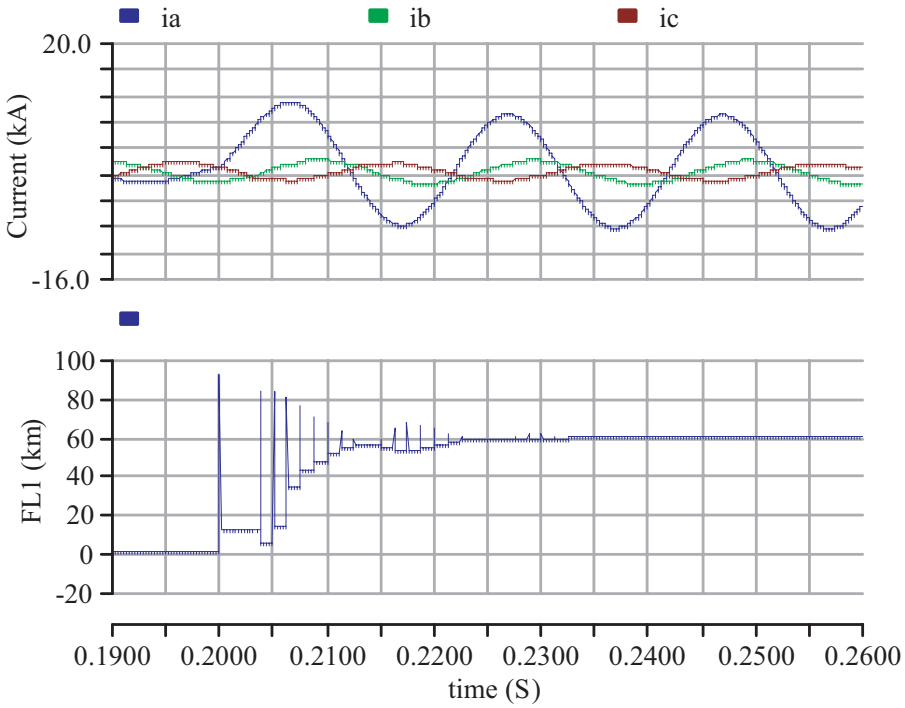

Figure 11. SPG with transition resistance $R_f = 30\,\Omega$.

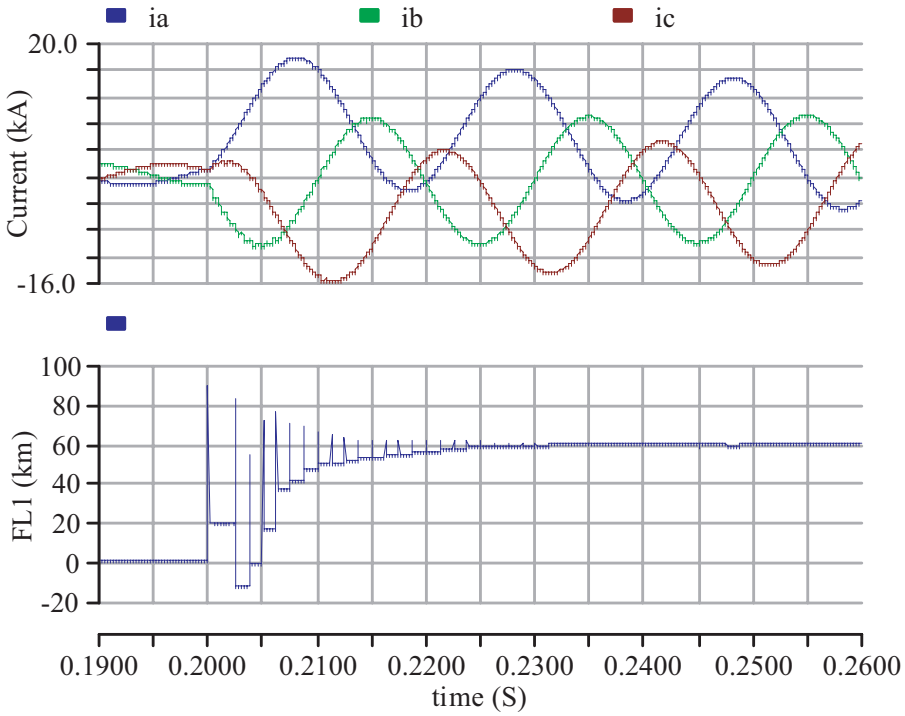

Figure 12. Metallic TPH.

circuit. For a 400 km line, the fault distance obtained by Equation (18) is 59.38 km. Figs. 13 and 14 respectively shows the fault location current and fault distance under a three-phase short circuit with transition resistance $R_f = 1\,\Omega$, $R_f = 5\,\Omega$. For the same 400 km line, the fault distance obtained by

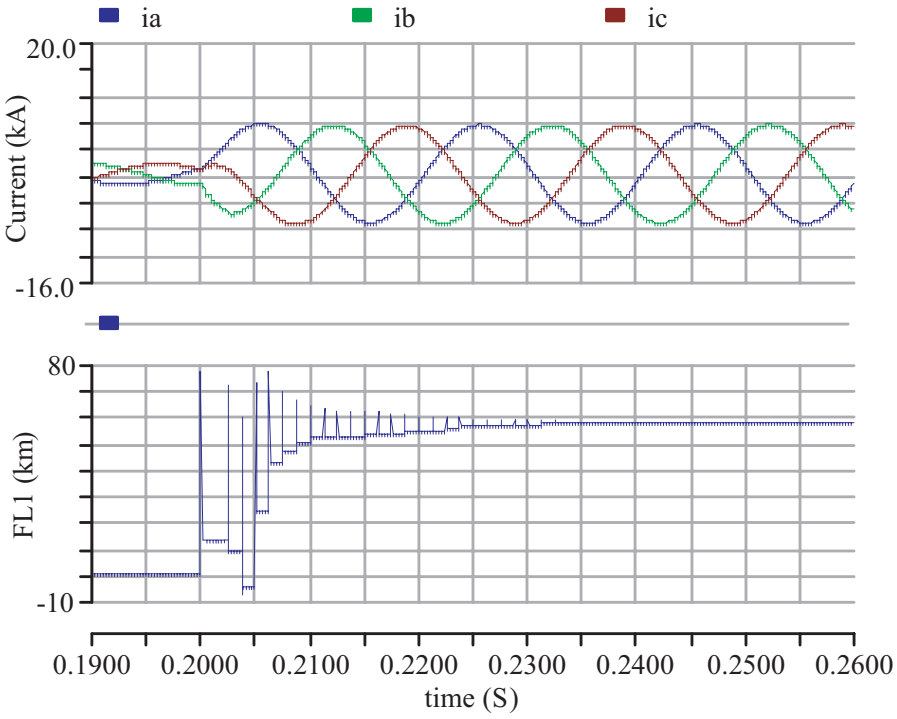

Figure 13. TPH with transition resistance $R_f = 1\,\Omega$.

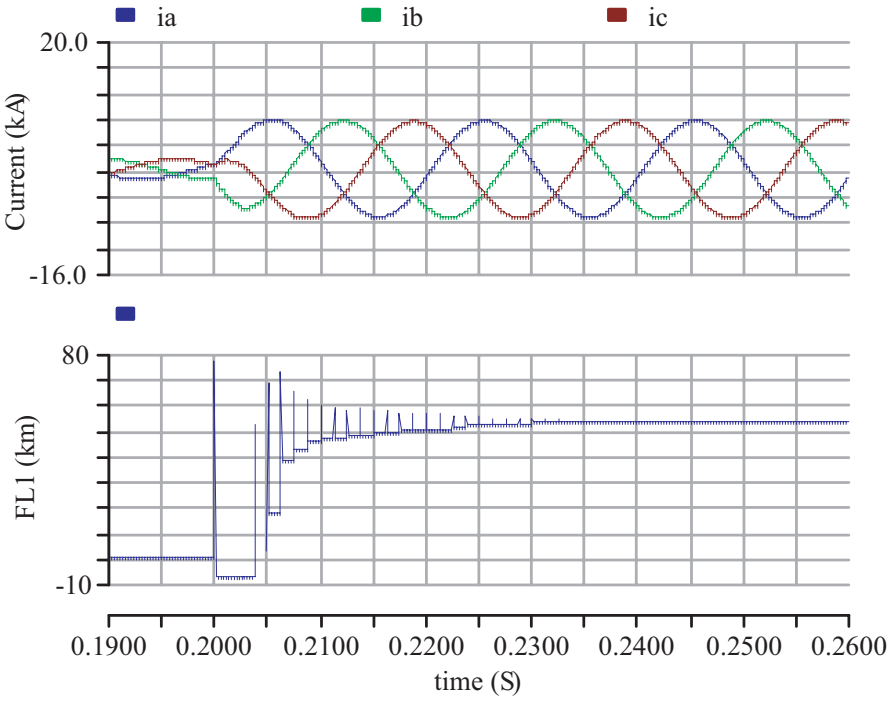

Figure 14. TPH with transition resistance $R_f = 5\,\Omega$.

Equation (18) is 57.85 km in Fig. 13.

When the distance to the fault is calculated with Equation (18), due to neglecting the fault resistance, for a metallic three-phase short circuit occurs, the result obtained by the algorithm is

accurate. At this time, the fault arc resistance is proportional to the arc length. In the case of a large fault current such as 10 kA, a small path resistance has little effect on the calculation of fault distance. However, high impedance will cause great errors in the calculation results of the algorithm.

In this study, the method of evaluating error is as follows [26]:

$$\text{Error } (\%) = \frac{|l_{\text{exact}} - l_{\text{est}}|}{D} \cdot 100\% \tag{19}$$

where l_{exact} is the actual location, l_{est} the estimated location, and D the length of the line.

Only 5% of power system short circuits are three-phase short circuits, of which the vast majority are human factors, and the dominant ones are metallic short circuits and arc short circuits. High impedance three-phase short circuits are quite rare. In this case, the simulation results will be given in Table 3.

Table 3. TPH error.

R_f [Ω]	Error (%) on different fault location			
	30 km	60 km	150 km	240 km
$R_f = 0$	0.0853	0.0984	0.0962	0.0952
$R_f = 0.25$	0.0923	0.1286	0.1562	0.2010
$R_f = 1$	0.6658	0.7852	0.5362	0.4538
$R_f = 2$	1.8594	1.1566	1.6952	1.8410
$R_f = 5$	2.6851	2.6852	3.0153	2.8651
$R_f = 10$	6.2674	7.5621	6.5920	7.9611

3.3. Effect of the Line Load Condition

In order to evaluate the algorithm in different load conditions, Tables 4 to 7 respectively give evaluation results under no-load and heavy-load.

Table 4. SPG.

load states	Fault location (km)	SPG	
		Est. (km)	Error (%)
no-load	30	30.48	0.120
	60	60.45	0.113
	150	151.68	0.420
	240	241.22	0.305
Heavy-load	30	31.82	0.455
	60	61.56	0.390
	150	151.68	0.420
	240	242.52	0.630

It can be seen that the algorithm proposed in this paper is not affected by the line load condition comparing the results in the two cases of heavy load or light load before the fault. The distance to fault calculated by the algorithm is only related to the fault point. When the distance to fault point is set to 30 km, 60 km, 150 km, and 240 km, respectively, the error percentage does not exceed 0.63.

3.4. Effect of Line Transposition Condition

In order to evaluate the effects of line transposition on the algorithm, for different types of faults, the results of the fault location algorithm in this paper are given. It can be seen from Tables 8 to 11 that

Table 5. DPG.

load states	Fault location (km)	DPG	
		Estmi FL (km)	Error of Estim FL (%)
no-load	30	30.39	0.098
	60	60.69	0.172
	150	151.25	0.313
	240	241.69	0.422
Heavy-load	30	31.56	0.390
	60	58.95	0.262
	150	148.65	0.337
	240	242.98	0.745

Table 6. DPH.

load states	Fault location (km)	DPH	
		Estmi FL (km)	Error of Estim FL (%)
no-load	30	30.27	0.067
	60	60.82	0.205
	150	151.16	0.290
	240	241.88	0.470
Heavy-load	30	31.94	0.485
	60	58.56	0.360
	150	151.85	0.462
	240	242.52	0.630

Table 7. TPH.

load states	Fault location (km)	TPH	
		Estmi FL (km)	Error of Estim FL (%)
no-load	30	30.34	0.085
	60	60.39	0.098
	150	150.37	0.092
	240	240.38	0.095
Heavy-load	30	30.33	0.083
	60	60.62	0.154
	150	150.65	0.162
	240	240.54	0.135

the algorithm proposed in this paper is not affected by the line transposition condition comparing the line transposition and untransposition.

3.5. Effect of Fault Inception Angle

In order to evaluate the effects of fault inception angle on the algorithm, for different types of faults, the results of the fault location algorithm are given on heavily loaded lines (i.e., a power angle difference of

Table 8. SPG.

load states	Fault location (km)	SPG	
		Est.(km)	Error (%)
transposition	30	30.88	0.22
	60	60.69	0.17
	150	151.45	0.36
	240	241.96	0.49
untransposition	30	31.96	0.49
	60	61.57	0.39
	150	151.46	0.37
	240	242.42	0.60

Table 9. DPG.

load states	Fault location (km)	SPG	
		Est.(km)	Error (%)
transposition	30	30.96	0.22
	60	60.52	0.13
	150	151.63	0.41
	240	241.42	0.35
untransposition	30	31.01	0.50
	60	58.99	0.25
	150	148.74	0.31
	240	242.28	0.57

Table 10. DPH.

load states	Fault location (km)	DPH	
		Est. (km)	Error (%)
transposition	30	30.55	0.14
	60	60.93	0.23
	150	151.56	0.39
	240	242.32	0.58
untransposition	30	32.03	0.51
	60	58.98	0.26
	150	151.80	0.45
	240	242.85	0.71

20°). It can be seen from Table 12. that the algorithm proposed is not affected by the fault inception angle. The path resistance in the case of an asymmetric fault is 20 Ω, and a three-phase fault is a metallic fault. The fault point is 100 km away from the sender. Inception angle is set to 0°, 45°, 90°, and 180°, respectively.

Table 11. TPH.

load states	Fault location (km)	TPH	
		Est. (km)	Error (%)
transposition	30	30.94	0.24
	60	60.89	0.22
	150	150.27	0.07
	240	241.08	0.27
untransposition	30	30.93	0.23
	60	60.52	0.13
	150	150.65	0.16
	240	240.79	0.20

Table 12. The effect of fault inception angle on the positioning result.

Fault Type	Inception angle (degrees)	Estmi (km)	Error (%)
SPG	0	101.52	0.380
	45	101.36	0.340
	90	101.3	0.325
	180	101.45	0.363
DPG	0	101.62	0.405
	45	101.49	0.372
	90	101.23	0.308
	180	101.69	0.422
DPH	0	101.05	0.262
	45	100.98	0.245
	90	100.96	0.240
	180	100.81	0.203
TPH	0	101.66	0.415
	45	101.42	0.355
	90	101.25	0.313
	180	101.58	0.395

4. CONCLUSIONS

This paper proposes a fault location algorithm based on fault sequence components that is independent of parameters. The algorithm is an extension of the fault location algorithm at both ends. Using PMU devices installed at both ends of the line, the algorithm collects current and voltage to complete synchronous information sampling. The fault location algorithm is suitable for asymmetric faults and symmetrical faults. It is not affected by zero sequence coupling. For asymmetric faults, it is not affected by the path resistance. The algorithm is simple and efficient, because it is not affected by fault type, fault starting angle, line transposition, and line load. The simulation results prove that the algorithm efficiently and accurately determines the fault location.

ACKNOWLEDGMENT

This work was supported in part by the National Natural Science Foundation of China under Grants 51777024, 61806126.

REFERENCES

1. Zhen, Y. X., G. Xu, and R. Li, "A new fault-impedance algorithm for distance relaying on a transmission line," *IEEE Trans. Power Del.*, Vol. 15, No. 2, 2328–2338, 2010.
2. Magnago, F. H., "Fault location using wavelets," *IEEE Trans. Power Del.*, Vol. 13, No. 2, 1475–1480, 1998.
3. Shu, H. C., X. H. Liu, and X. C. Tian, "Single-ended fault location for hybrid feeders based on characteristic distribution of traveling wave along a line," *IEEE Trans. Power Del.*, Vol. 36, No. 1, 339–350, 2021.
4. Girgis, A., D. Hart, and W. Peterson, "A new fault location technique for two- and three-terminal lines," *IEEE Trans. Power Del.*, Vol. 7, No. 3, 98–107, 1992.
5. Cozza, A. and Y. Z. Xie, "Surge compression for improved fault location accuracy in full transient-based methods," *IEEE Sensors Journal*, Vol. 21, No. 2, 995–1008, 2021.
6. Rui, F., Y. Liu, R. S. Diao, and S. B. Wang, "Precise fault location on transmission lines using ensemble Kalman filter," *IEEE Trans. Power Del.*, Vol. 33, No. 4, 3252–3256, 2018.
7. Kumar, A. N., C. Sanjay, and M. Chakravarthy, "Fuzzy inference system-based solution to locate the cross-country faults in parallel transmission line," *International Journal of Electrical Engineering Education*, Vol. 58, No. 1, 83–96, 2021.
8. Kang, N. and J. X. Chen, "A fault-location algorithm for series-compensated double-circuit transmission lines using the distributed parameter line model," *IEEE Trans. Power Del.*, Vol. 32, No. 3, 2398–2407, 2017.
9. Gopalakrishnan, D., M. Hamai, and S. McKenna, "Fault location using the distributed parameter transmission line model," *IEEE Trans. Power Del.*, Vol. 15, No. 8, 1169–1174, 2000.
10. Karcius, M., K. M. Dantas, K. M. Silva, and K. M. Flavio, "Accurate two-terminal transmission line fault location using traveling waves," *IEEE Trans. Power Del.*, Vol. 33, No. 3, 873–880, 2018.
11. M. Kezunovic, B. Perunicic, Automated transmission line fault analysis using synchronized sampling at two ends. *IEEE Trans. Power Del.*, Vol. 11, No. 5, 121-129, 1988.
12. Ghorbani, A. and H. Mehrjerdi, "Negative-sequence network based fault location scheme for double-circuit multi-terminal transmission lines," *IEEE Trans. Power Del.*, Vol. 34, No. 3, 1109–1117, 2019.
13. Dobakhshari, A. S. and M. Ranjbar, "A novel method for fault location of transmission lines by wide-area voltage measurements considering measurement errors," *IEEE Trans. Smart Grid*, Vol. 6, No. 5, 874–884, 2015.
14. Dobakhshari, A. S., "Wide-area fault location of transmission lines by hybrid synchronized/unsynchronized voltage measurements," *IEEE Trans. Smart Grid*, Vol. 9, No. 3, 186–192, 2018.
15. Azizi, S. and S. M. Pasand, "Fault location on multiterminal DC systems using synchronized current measurements," *Int. J. Elect. Power Energy Syst.*, Vol. 64, 779–786, 2014.
16. Zhang, C. H., G. B. Song, and L. M. Yang, "Time-domain single-ended fault location method that does not need remote-end system information," *IET Generation Transmission & Distribution*, Vol. 14, No. 2, 284–293, 2020.
17. Preston, G., M. Radojevic, H. Kim, and V. Terzija, "New settings-free fault location algorithm based on synchronized sampling," *IET Generation Transmission & Distribution*, Vol. 5, No. 2, 376–383, 2011.
18. Jiang, J. A., Y. H. Lin, C. W. Liu, and J. C, Ma, "An adaptive PMU based fault detection/location technique for transmission lines part I: Theory and algorithms," *IEEE Trans. Power Del.*, Vol. 15, No. 3, 486–493, 2000.

19. Liao, Y., "Fault location for single-circuit line based on bus-impedance matrix utilizing voltage measurements," *IEEE Trans. Power Del.*, Vol. 23, No. 5, 609–617, 2008.
20. Yu, C. S., C. W. Liu, and S. L. Yu, "A new PMU-based fault location algorithm for series compensated lines," *IEEE Trans. Power Del.*, Vol. 17, No. 2, 33–46, 2002.
21. Liao, Y. and S. Elangovan, "Unsynchronized two-terminal transmission line fault-location without using line parameters," *IEE Proc. Gener. Transmiss. Distrib.*, Vol. 153, 639–643, 2006.
22. Feng, G. and A. Abur, "Fault location using wide-area measurements and sparse estimation," *IEEE Trans. Power Syst.*, Vol. 31, No. 4, 2938–2945, 2016.
23. Zhao, L. H., J. W. Zhu, and B. Gu, "A new technique based on fundamental frequency positive sequence fault components for fault location," *IEEJ Transactions on Electrical and Electronic Engineering*, Vol. 15, 536–543, 2020.
24. Zhang, Y., J. Liang, Z. Yun, and X. M. Dong, "A new fault-location algorithm for series-compensated double-circuit transmission lines based on the distributed parameter model," *IEEE Trans. Power Del.*, Vol. 33, No. 2, 3249–3251, 2018.
25. Liao, Y., "Transmission line fault location algorithms without requiring line parameters," *Elect. Power Compon. Syst.*, Vol. 11, No. 11, 1218–1225, 2008.
26. IEEE Guide for Determining Fault Location on AC Transmission and Distribution Lines, IEEE Standard C37.114TM-2004, 2005.